Available online at www.sciencedirect.com
SCIENCE DIRECT
Polymer 46 (2005) 11600–11609
polymer
www.elsevier.com/locate/polymer

Investigation on the polyamide 6/organoclay nanocomposites with or without a maleated polyolefin elastomer as a toughener

Fang-Chyou Chiu [a], Sun-Mou Lai [b,*], Yu-Lun Chen [a], Tsung-Han Lee [a]

[a] Department of Chemical and Materials Engineering, Chang Gung University, Tao-Yuan 333, Taiwan, ROC
[b] Department of Chemical and Materials Engineering, National I-Lan University, I-Lan 260, Taiwan, ROC

Received 6 July 2005; received in revised form 24 September 2005; accepted 26 September 2005
Available online 20 October 2005

Abstract

Polyamide 6 (PA 6)-based nanocomposites were prepared using a melt-mixing technique in this study. One commercial organoclay (denoted 30B) and one maleated polyolefin elastomer (denoted POEMA) served as the reinforcing filler and toughener, respectively. The X-ray diffraction (XRD), scanning electron microscopy combined with energy dispersive spectroscopy (SEM/EDS) and transmission electron microscopy (TEM) results confirmed the nano-scaled dispersion of 30B in the composites. Different mixing sequences presented similar phase morphology for the same formulated nanocomposites. XRD results also revealed that both 30B and POEMA would induce the formation of γ form PA 6 crystal, with 30B exhibiting a higher efficiency. Differential scanning calorimetry (DSC) results indicated that the addition of 30B altered the crystallization kinetics of PA 6, which was mainly attributed to the prevailing formation of γ form crystal. Complex melting behaviors were observed for neat PA 6 and the nanocomposites. These complex behaviors are associated with different polymorphs and the 'melting-recrystallization-remelting' phenomenon. Moderate thermal stability enhancement of PA 6 after adding 30B and/or POEMA was confirmed using thermogravimetric analysis (TGA). The storage modulus, Young's modulus and tensile strength of PA 6 were increased after adding 30B. However, these properties declined after further incorporation of POEMA. The different-processed PA 6/30B/POEMA nanocomposites displayed balanced tensile properties and toughness between those of neat PA 6 and PA 6/30B nanocomposite.

Keywords: PA 6; Organoclay; Nanocomposite

1. Introduction

In the past decade, researches on the preparation and characterization of organic-inorganic nanocomposites have attracted much academic and industrial attention. Among the nanocomposites investigated, polymer/clay (silicate) systems have exhibited great promise for industrial applications due to their potential to display synergistically advanced properties with only minor amounts (e.g. 3–5 wt%) of clay loading. The typical enhanced properties include tensile/flexural strength, heat deflection temperature (HDT), thermal stability, flame retardancy, barrier property and so on. The successful pioneering work on these nanocomposites was conducted on the polyamide 6 (PA 6)/montmorillonite (MMT) clay system by Toyota Inc. [1,2]. Since then, the anticipated versatile applications have led to vigorous researches on other polymer/clay nanocomposite systems, in which the polymeric matrix includes polyolefins [3–6], epoxy [7], polyesters [8–11], polyamides [12–14], styrenic polymers [15,16], polyurethanes [17], etc.

MMT was recognized as an appropriate choice for preparing high performance polymer/clay nanocomposites. This naturally occurring clay displays a hydrophilic layered-structure, comprised of 1-nm thin individual layers. These layers assemble themselves via specific interactions in a parallel manner to form a stacked (tactoid-like) arrangement in the micrometer scale. Because of the MMT's hydrophilic features, little difficulty should be encountered using polar polymers to develop MMT-based nanocomposites, if the MMT surface is modified with certain organic surfactants (e.g. alkylammonium cation, the modified MMT is thus denoted O-MMT in the following) [10,13]. The incorporation of organic surfactants will expand the MMT's interlayer spacing and offer a positive enthalpic effect for mixing.

PA 6 is a polar polymer and is used in numerous engineering applications due to its versatile properties. However, some drawbacks remain to be improved, such as

* Corresponding author. Tel.: +886 3 935 7400x710; fax: +886 3 935 7025.
E-mail address: smlai@niu.edu.tw (S.-M. Lai).

0032-3861/$ - see front matter © 2005 Elsevier Ltd. All rights reserved.
doi:10.1016/j.polymer.2005.09.077

low HDT and brittleness. Proper fillers and/or reinforcements are commonly incorporated into the PA 6 matrix to improve its properties. Recently, several studies on the melt-mixed PA 6/clay (nano)composites have been carried out. For example, Liu et al. [18] reported that due to the nano-scale effects and the strong interaction between PA 6 and O-MMT, the crystal form and crystallization behavior of PA 6 were influenced. The γ form crystal formation of PA 6 was promoted in the nanocomposites. Fornes et al. [19] studied the PA 6 molecular weight effect on the properties of PA 6/O-MMT nanocomposites. They found that O-MMT was dispersed more uniformly in a higher molecular weight PA 6 matrix, which conferred better mechanical property performance. Cho and Paul [20] confirmed that the twin screw extruder is a better mixing equipment for PA 6/organoclay nanocomposite preparation than the single screw extruder. Comparisons between the PA 6/organoclay nanocomposite and conventional PA 6/glass fiber composite mechanical properties were also made. Liu et al. [21] also investigated the morphology and mechanical properties of PA 6/organoclay nanocomposites. The PA 6 γ form crystals were verified to be induced by the addition of an organoclay. As the organoclay load increased, the tensile modulus and yield strength of the nanocomposites increased, while the strain-at-yield decreased. Lincoln et al. [22] studied the crystalline morphology of PA 6/O-MMT nanocomposites in detail. They found that the presence of O-MMT stabilized the dominant γ form PA 6 crystals during the heating process. The lamellar stack morphology versus temperature for PA 6 and its nanocomposites was also revealed. The nonisothermal crystallization behavior of PA 6/O-MMT nanocomposites was explored by Tjong and Bao [23]. Several models were used to analyze the experimental data. The folded surface energy of PA 6 crystals was found not to be influenced by the existence of O-MMT. More recently, some PA 6-based blend/organoclay nanocomposites were investigated [24–27].

From the aforementioned literature, it was found that PA 6/organoclay nanocomposites could exhibit superior stiffness and heat resistance over neat PA 6. Nevertheless, the impact strength (toughness) of PA 6 generally declined after adding organoclays. It is recognized that the toughening of PA 6 can be achieved by incorporating a low-modulus second component (e.g. elastomers). Among the elastomers used, recently maleated metallocene polyolefin elastomers (POEs) were found to effectively enhance PA 6 toughness [28,29]. To our best knowledge, little work was conducted on the toughening of PA 6/clay nanocomposites. The aim of this work is to evaluate the combined effects of adding an organoclay and a maleated metallocene POE toughener on PA 6/clay nanocomposites preparation and their thermal/mechanical properties. In this study, one commercially available O-MMT and one maleic anhydride-grafted POE (POEMA) were used to melt-mix with PA 6. The effect of different mixing sequences on the morphology and properties of the prepared nanocomposites was assessed as well.

2. Experimental section

The PA 6 (trade name TP 4208) used in this study is a commercial product of Zig Sheng Industrial Co., Taiwan. Its relative viscosity is 2.43. An O-MMT clay (Cloisite® 30B, denoted 30B) obtained from Southern Clay Products, Inc. was used as the nano-filler for composites preparation. As informed by the manufacturing company, the organic modifier for 30B is a methyl tallow bis-2-hydroxyethyl quaternary ammonium ion. The tallow composition is ca. 65% C18, 30% C16, and 5% C14. A POEMA with 1 wt% of MA, supplied by Nytex Composites Co. (Taiwan), was used as the toughener for the PA 6/30B composite prepared. The POEMA possesses a melt flow index of 9.1 g/10 min (at 230 °C and 2.16 kg load); the POE portion is a product (Engage® 8180) of Dupont Dow Elastomer Co.

All composites were prepared using a melt-mixing procedure through a Haake Rheomex intermeshing twin-screw extruder (length = 1100 mm, $L/D = 44$) in the corotating mode. The screw speed was maintained at 200 rpm. The barrel temperature was kept in the 230–250 °C range. Before melt-mixing, the ingredients were dried for 24 h in an air-circulated oven to remove the absorbed water. The 30B content of the composites was kept at 5 wt%. The POEMA was loaded at 10 wt% if needed. Basically, a one-step mixing process was carried out for the composites preparation. The ingredients were weighed at a certain ratio and then dry-mixed as one before feeding into the extruder. For composites with POEMA inclusion, a two-step mixing process was additionally carried out to check the effect of different mixing sequences on the prepared composite properties. In the two-step mixing process, PA 6 was melt-mixed with either 30B or POEMA first. Afterward the extrudate was further meltmixed with the other ingredient. After melt-mixing, the extruded materials were pelletized, followed by oven-drying before further characterization. For comparison purposes, neat PA 6 was melt-extruded under the same condition. The formulation and sample designations for the manufactured composites are listed in Table 1.

X-ray diffraction (XRD) technique, scanning electron microscopy combined with energy dispersive spectroscopy (SEM/EDS) and transmission electron microscopy (TEM) were employed to assess the dispersibility of 30B in the composites. PA 6 crystal form of different thermally treated samples was determined by XRD as well. A Siemens D5005

Table 1
Samples designation and formulations

Designation	Composition	Parts (wt%)
PA 6	PA 6	100
PA 6/POEMA	PA 6/POEMA	90/10
PA 6/30B	PA 6/30B	95/5
PA 6/30B/POEMA	PA 6/30B/POEMA	85/5/10
PA 6/30B*/POEMA	PA 6/30B/POEMA	85/5/10
PA 6/30B/POEMA*	PA 6/30B/POEMA	85/5/10

*The asterisk-included samples were prepared through a two-step mixing process; the ingredient with asterisk was mixed with PA 6 at the first step.

X-ray unit operating at 40 kV and 30 mA was used to carry out the XRD experiments at room temperature. The X-ray source was CuK_α radiation with a wavelength of 0.154 nm. The diffractograms were scanned at 2θ range from 1.5 to 30° at a rate of 0.01°/s. The SEM/EDS experiments were performed on fractured surfaces of the samples with a combined JEOL JSM-5410 and JEOL 6587 system. The TEM observations were performed on ultrathin sections of cryo-microtomed thin composite films with a JEOL JEM-2000EX II system using an acceleration voltage of 100 kV.

The crystallization and melting behaviors of the samples were measured using a Perkin–Elmer DSC 7 analyzer equipped with an intra-cooler. The heat flow and temperature of the instrument were calibrated using standard materials, such as indium and zinc. During the crystallization experiments, the specimens were first melted at 250 °C for 5 min, and then cooled to room temperature at different rates. The crystallized specimens were subsequently heated at different rates for the corresponding melting behavior investigations. The thermal stability of the samples was characterized using a thermo-gravimetric analyzer (TGA) on a TA Instruments TGA 2050 system under a nitrogen environment. The heating process was conducted from room temperature to 700 °C at a rate of 40 °C/min.

The dynamic mechanical properties of compression-molded specimens were measured using a Perkin–Elmer DMA 7e system. The measurements were carried out in the three-point bending mode under a 10 °C/min rate at a frequency of 1 Hz in an air atmosphere. Tensile properties of dog-bone-shaped specimens (according to ASTM D638) were determined using a MTS Sintech 5/G system. Young's modulus, tensile strength and elongation at break were recorded at a crosshead speed of 17 mm/min (0.5 strain rate). Notched Izod impact test was performed using a CEAST impact tester in accordance with ASTM D256. The tensile properties and impact strength reported were averaged values from at least five specimens of the same sample.

3. Results and discussion

3.1. Dispersibility of 30B in the composites

According to the dispersion status of layered clays in the polymeric matrix, three types of composites can be classified: (1) conventional macrocomposites, (2) partially exfoliated composites, including intercalated clays, and (3) fully exfoliated nanocomposites. XRD is a widely employed technique for characterizing the clay dispersibility. Fig. 1 shows the XRD patterns of neat 30B and the composites (in the 2θ range $<10°$). As seen, the characteristic (001) diffraction peak of neat 30B locates evidently around $2\theta = 4.9°$ (d-spacing: 1.80 nm), but no discernible peak of 30B is observed for the composites. This result suggests the interlayer spacing of 30B was mostly expanded over 5.88 nm or the layered-structure of 30B hardly existed in the composites. Certainly, no differences in the 30B dispersibility were detected for different composites. The exfoliation and/or intercalation of 30B should have taken

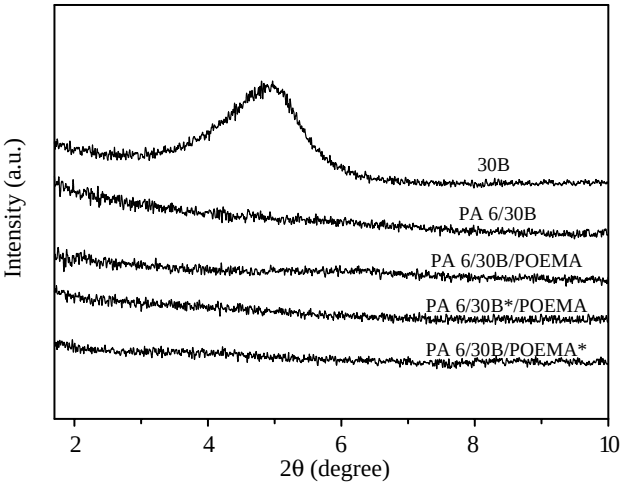

Fig. 1. XRD patterns of 30B and the prepared composites.

place during the melt-mixing processes. To further verify the dispersion status of 30B in the composites, SEM/EDS experiments were carried out. Fig. 2(a) and (b) illustrate the representative SEM micrographs of PA 6/30B composites with and without (w/o) POEMA inclusion. It is shown that no 30B aggregates were observed within the two samples. Due to the compatibility between PA 6 and POEMA, the POEMA phase was indiscernible within the PA 6 matrix as well. Fig. 2(c) and (d) depict the corresponding EDS Si mapping results for the two samples. The light spots indicate the locations of Si element (from 30B). These spots were found to be randomly distributed within the samples irrespective of the existence of POEMA or not. The 30B is thus suggested to be dispersed homogeneously in the composites [30]. For different-processed PA 6/30B/POEMA composites, their SEM/EDS results were similar to one another (not shown here for brevity). Additionally, from all the SEM observations, it was noted that the addition of 30B hardly changed the compatibility between PA 6 and POEMA. The dispersion status variation of POEMA in PA 6 was undetectable.

TEM experiments can provide more detailed dispersion status for 30B in the composites. Fig. 3 displays TEM micrographs of the representative composites. The dark lines represent 30B; the white/gray base represents the polymer phase. In Fig. 3(a) (cf. PA 6/30B composite), the 30B was observed to be partially exfoliated into a thinner multi-layered structure or even single layer, indicating a nano-scaled dispersion was achieved. Accordingly, no discernable (001) diffraction was observed in the corresponding XRD pattern. Fig. 3(b) and (c) shows the dispersion status of 30B in POEMA-included composites prepared via different processes. Note that the morphology of the two composites resemble each other, indicating that different mixing processes affected the 30B dispersibility to a limited extent. A similar morphology is also observed in another POEMA-included composite. While comparing the morphology of composites w/o POEMA inclusion, it was revealed that the addition of POEMA hardly altered the 30B dispersibility in the composites. 30B seemed to be randomly distributed in the PA 6 and POEMA phases.

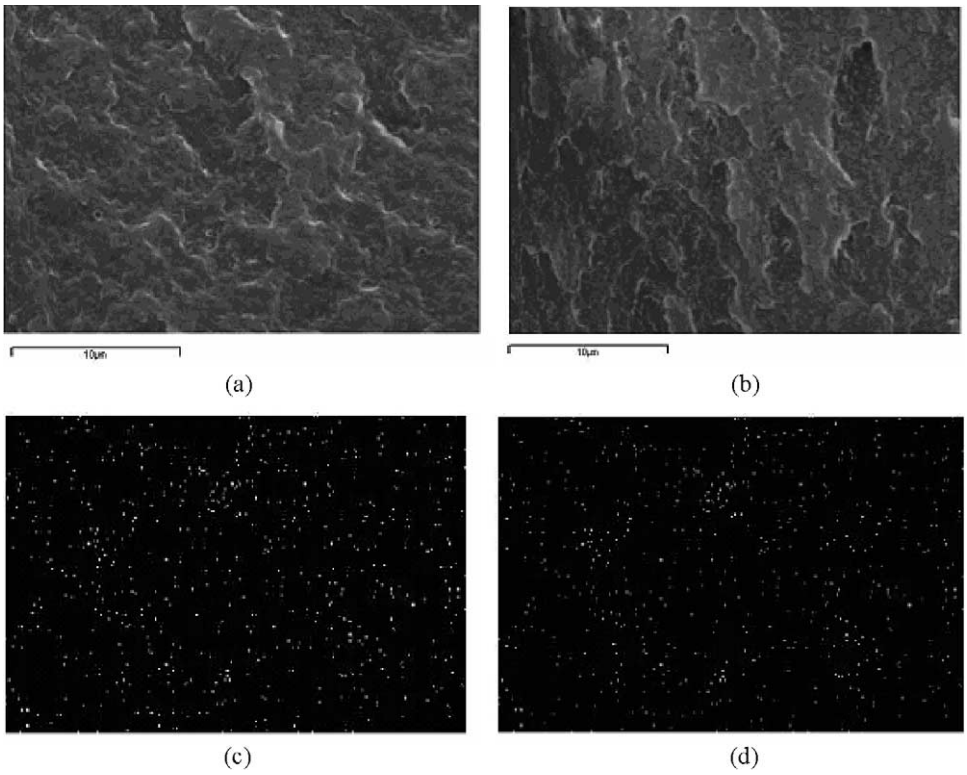

Fig. 2. (a) SEM micrograph of PA 6/30B composite; (b) SEM micrograph of PA 6/30B/POEMA composite; (c) EDS Si mapping of PA 6/30B composite; (d) EDS Si mapping of PA 6/30B/POEMA.

This result implies 30B is not only compatible with PA 6 but also shows some affinity to POEMA. The compatibility between PA 6 and 30B is well recognized. The reason for POEMA showing compatibility with 30B could be attributed to its hydrophilic MA portion characteristic. Through the 30B dispersibility observations, it can be concluded that various PA 6-based nanocomposites were developed.

3.2. Crystal structure

PA 6 has been reported to exhibit two dominant monoclinic crystalline forms, termed α and γ. The α form consists of all-*trans* chain conformation, and the hydrogen bonds are formed between adjacent antiparallel chains (resulting in the *ac*-plane sheets). In the γ form, the chains are instead twisted to allow hydrogen bonds formation between parallel chains. The formation of these two forms depends mainly on the crystallization conditions or the additions of specific fillers. The α form is recognized as the most thermodynamically stable. The characteristic XRD peaks of the α form at room temperature are located around $2\theta = 21$ and 24°, and indexed as (200) and (002)/(202) diffractions, respectively [31]. For the γ form, the peaks show up around 11, 22 and 23°. They are diffractions from (020), (001) and (200)/($\bar{2}$01), respectively. Fig. 4 shows the XRD patterns of thermally treated samples in the 2θ range of 14–30°. Two main features are noteworthy in the figure. First, when the samples were cooled at 5 °C/min (Fig. 4(a)), neat PA 6 exhibited predominantly the α form structure, whereas PA 6/POEMA blend showed a mixed structure with a higher α form proportion, and all the nanocomposites induced huge γ form diffractions. Second, as the samples were cooled at higher rates (Fig. 4(b) and (c)), the intensities of γ form diffractions became relatively stronger. Particularly, this phenomenon is more evident for PA 6/POEMA blend. The first observation means that O-MMT (30B) induces the PA 6 γ form formation as reported and that POEMA could do so as well. That is, the original intra-sheet hydrogen bonds formation in α form crystal was disturbed by the additions of 30B and/or POEMA. However, the POEMA's efficiency in promoting the γ form development is less than that of 30B, which might be caused by the inferior dispersion status (less interaction) of POEMA within PA 6 matrix. The second observation indicates that the γ form is kinetically more favorable than the α form. A faster cooling rate facilitates γ form development as expected. Further noted in these figures is that the intensities of (200)/($\bar{2}$01) diffractions (shoulder of (001)) of γ form crystals became weaker as the cooling rate increased. This result suggests that some modification on the growth planes of γ form crystals occurred as the cooling rate changed. Moreover, the polymorph differences among the PA 6/30B nanocomposite and different-processed PA 6/30B/POEMA nanocomposites were not visible.

3.3. Crystallization and melting behaviors

As revealed from the above XRD results, the crystal form of PA 6 matrix was influenced with the inclusions of 30B and/or POEMA. Accordingly, these influences should be reflected

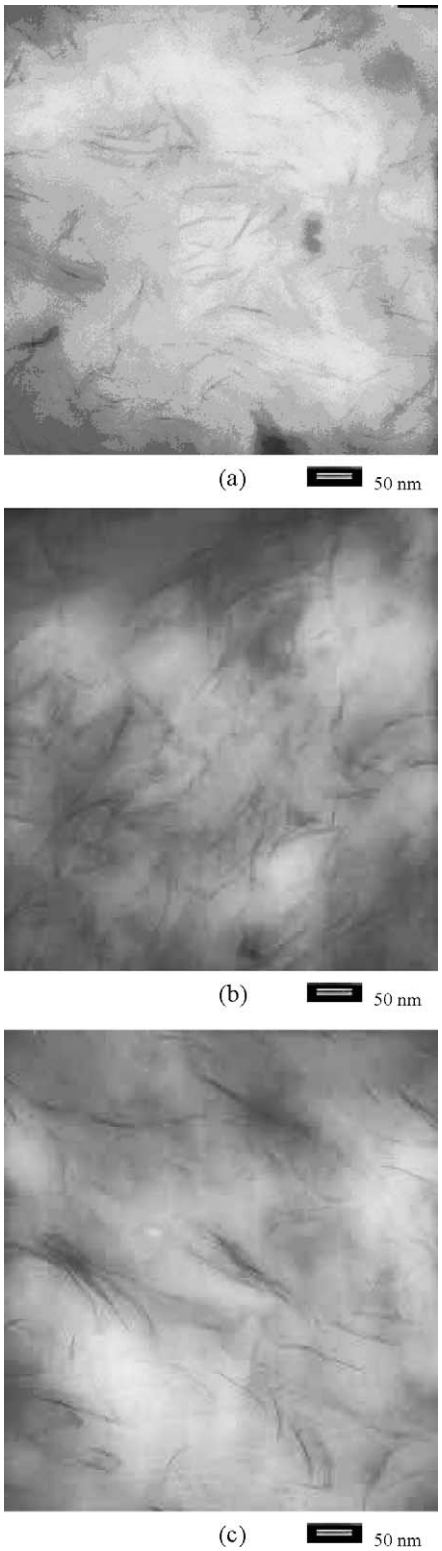

Fig. 3. TEM micrographs of the composites: (a) PA 6/30B; (b) PA 6/30B/POEMA; (c) PA 6/30B/POEMA*.

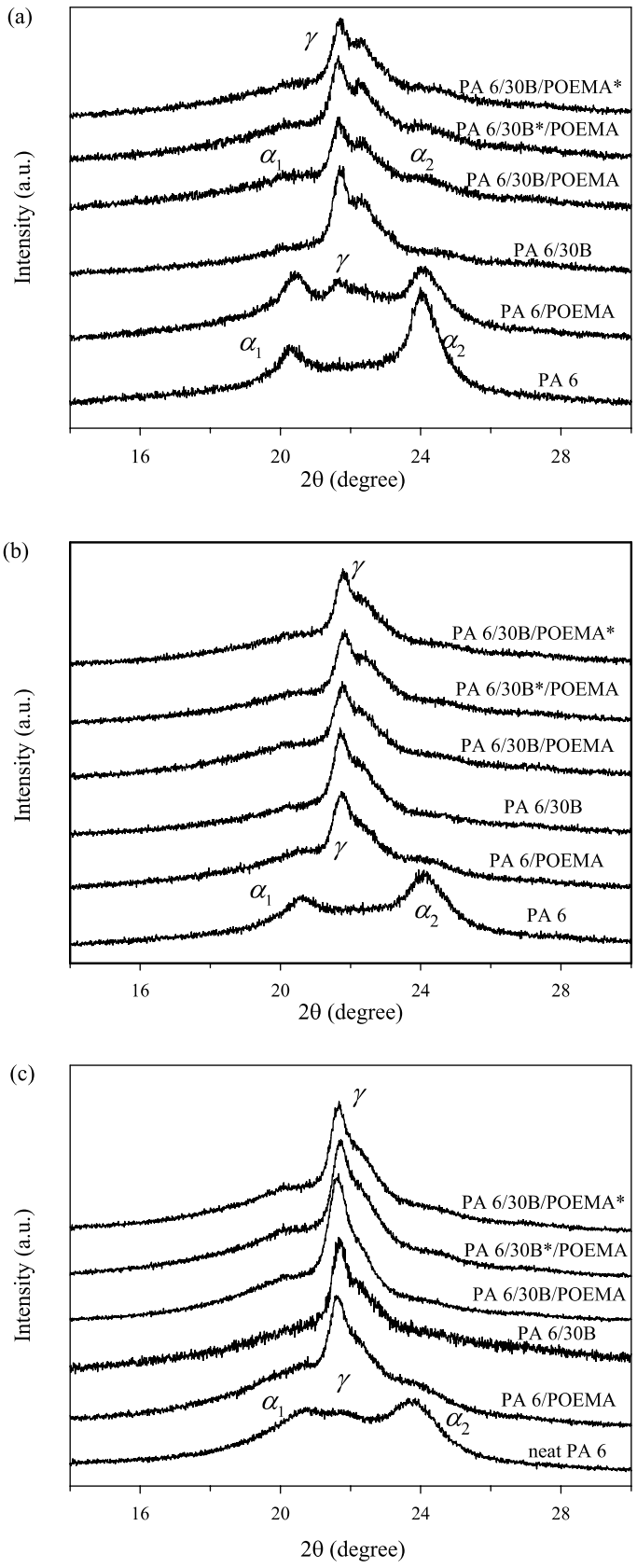

Fig. 4. XRD patterns of the samples cooled from the melt: (a) at 5 °C/min; (b) at 40 °C/min; (c) by air-quenching.

from the crystallization and melting behaviors of the samples. Fig. 5(a) shows the DSC cooling thermograms of the samples at a 5 °C/min rate. It was found that the crystallization peak temperature (T_p, temperature at the exotherm minimum) of either neat PA 6 or its blend was around 192–193 °C, whereas

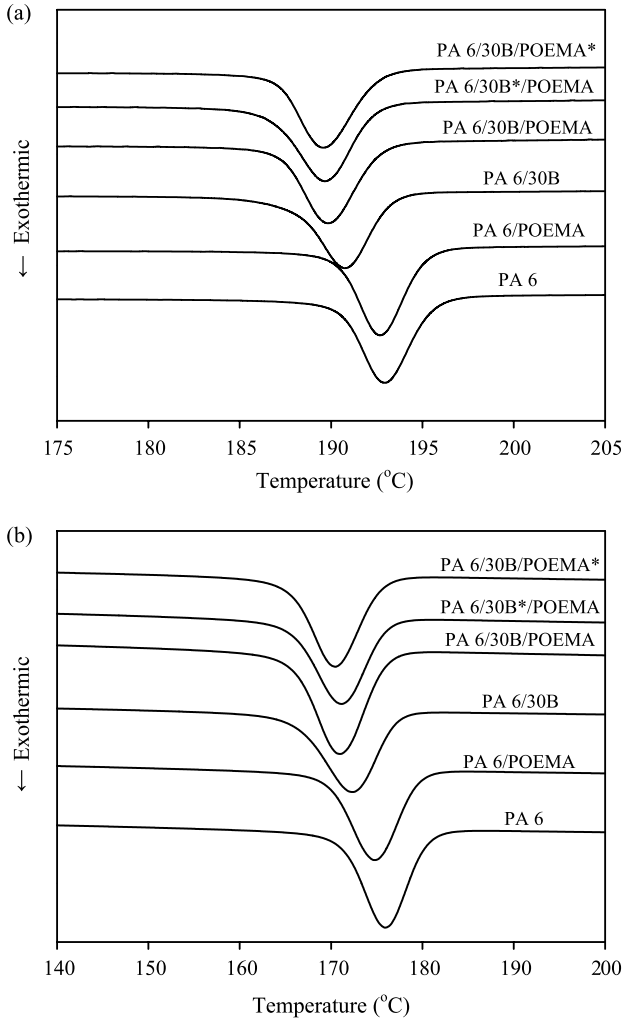

Fig. 5. DSC cooling thermograms of the samples: (a) at 5 °C/min cooling rate; (b) at 40 °C/min cooling rate.

the T_ps of nanocomposites shifted to approximately 189–190 °C. POEMA thus influenced the PA 6 crystallization kinetics slightly, but 30B evidently altered the PA 6 crystallization kinetics. A similar role that the organoclay played was reported in other PA 6 nanocomposite system [21]. According to the crystal structure results, the shifts of T_p to lower temperatures could mainly be attributed to the formation of γ form crystals. Nevertheless, a higher degree of interaction between the 30B platelets and PA 6 molecules occurred, causing impeded chain mobility in PA 6 upon crystallization. This should also have played a role in the observation. Hereby, the accelerating nucleation effect of 30B on PA 6 crystallization was obscured and not seen. Additionally, the crystallization enthalpy (ΔH_c) of PA 6 was found to increase for the PA 6/30B nanocomposite. As POEMA was further added into the nanocomposite, ΔH_c of PA 6 decreased. For the samples cooled at the rate of 40 °C/min (Fig. 5(b)), similar behaviors are observed, except the T_ps shift to lower temperatures. The T_ps and ΔH_cs of PA 6 in the samples are included in Table 2.

Fig. 6 shows the DSC heating thermograms of air-quenched samples (from 250 °C) under the rates of 40 and 5 °C/min,

Table 2
Some representative thermal and mechanical data of the samples

Properties	Samples					
	PA 6	PA 6/ POEMA	PA 6/ 30B	PA 6/ 30B/ POEMA	PA 6/ 30B*/ POEMA	PA 6/30B/ POEMA*
T_p (°C)[a]	193.0	192.7	190.5	189.8	189.7	189.6
ΔH_c (J/g)[a]	64.4	63.9	70.8	55.8	54.1	58.6
T_p (°C)[b]	175.9	174.5	172.8	171.2	171.0	170.7
ΔH_c (J/g)[b]	59.9	60.6	66.6	52.4	53.9	53.4
$T_{m,1}$ (°C)[c]	221.6	221.1	222.1	222.2	220.8	220.8
$T_{m,2}$ (°C)[c]	212.0	211.2	211.8	211.9	210.9	210.6
ΔH_m (J/g)[c]	61.6	51.7	54.5	53.2	51.3	52.6
T_{max} (°C)	460	465	466	470	467	468
YM (GPa)[d]	1.3	1.1	2.0	1.4	1.5	1.5
TS (MPa)[e]	47.3	43.1	75.2	48.2	50.5	51.6
EB (%)[f]	102	80	5	28	33	27
IS (J/m)[g]	37.7	104.8	22.8	51.6	63.7	51.8

[a] 5 °C/min-cooled.
[b] 40 °C/min-cooled.
[c] Air-quenched samples followed by 5 °C/min heating.
[d] Young's modulus.
[e] Tensile strength.
[f] Elongation at break.
[g] Izod impact strength.

respectively. Complex melting behaviors are observed. While heating at 40 °C/min, one major peak with a shoulder on the right-hand side located around 213 and 221 °C, respectively, exist for the nanocomposites and the blend (denoted nanocomposites/blend). According to the reports [18,21], the high melting temperature shoulder (denoted $T_{m,1}$) is associated with the α form crystals. The dominant low melting temperature peak (denoted $T_{m,2}$) belongs to the γ form crystals. The results suggest α and γ form crystals coexisted in the nanocomposites/blend, in which γ form was predominant. For neat PA 6, a major α form peak along with a trivial γ form endotherm is observed, indicating a α form dominant crystalline phase. In general, the DSC results are in agreement with the XRD data, except DSC results show a higher α form fraction in the nanocomposites/blend. This discrepancy can be attributed to the recrystallization/organization of α form crystals upon the heating scans. The shallow exotherm around 198 °C for the blend is evidence. This explanation can be further justified by examining the melting behaviors of the same samples heated at a slower rate (Fig. 6(b)). As the heating rate decreases, the relative $T_{m,1}$ peak intensity of the nanocomposites/blend increases. This means that more α form crystals would grow at a slower heating rate. The shallow exotherms prior to the apparent melting peaks are more discernible. In fact, we believe that the shallow exotherms result mainly from the overlapping effects of melting the original less stable α form crystals (endotherm, formed during the cooling process) and recrystallizing the more stable α form crystals (exotherm). Therefore, the $T_{m,1}$ peak associated crystals were formed at least partially during the heating process. The so-called 'melting-recrystallization-remelting' phenomenon occurred for the air-quenched samples. Inevitably, because of melting and recrystallization peaks crowding,

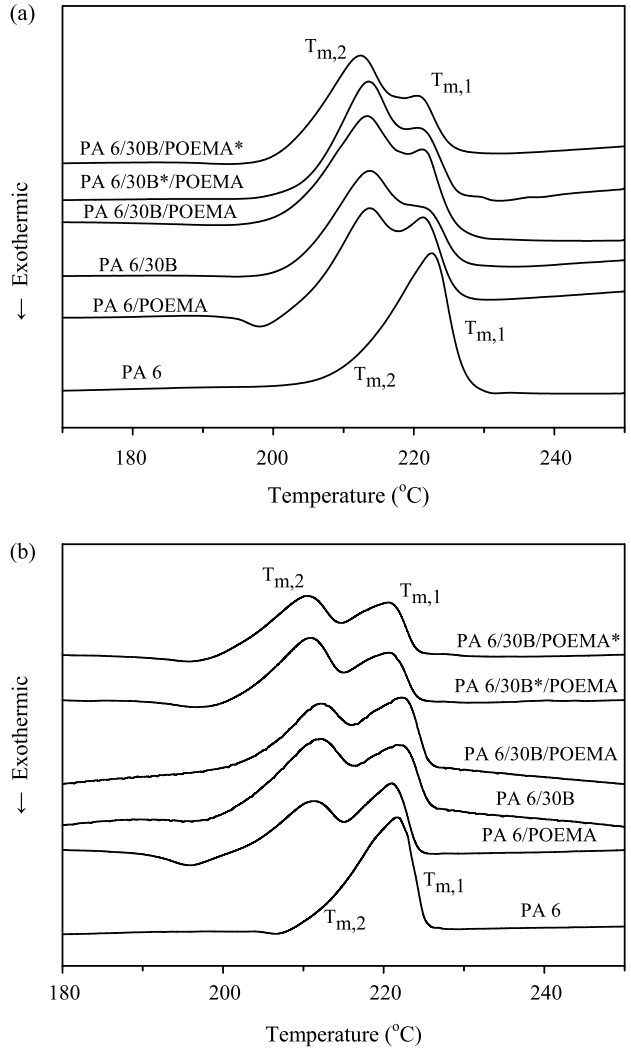

Fig. 6. DSC heating thermograms of air-quenched samples: (a) at 40 °C/min heating rate; (b) at 5 °C/min heating rate.

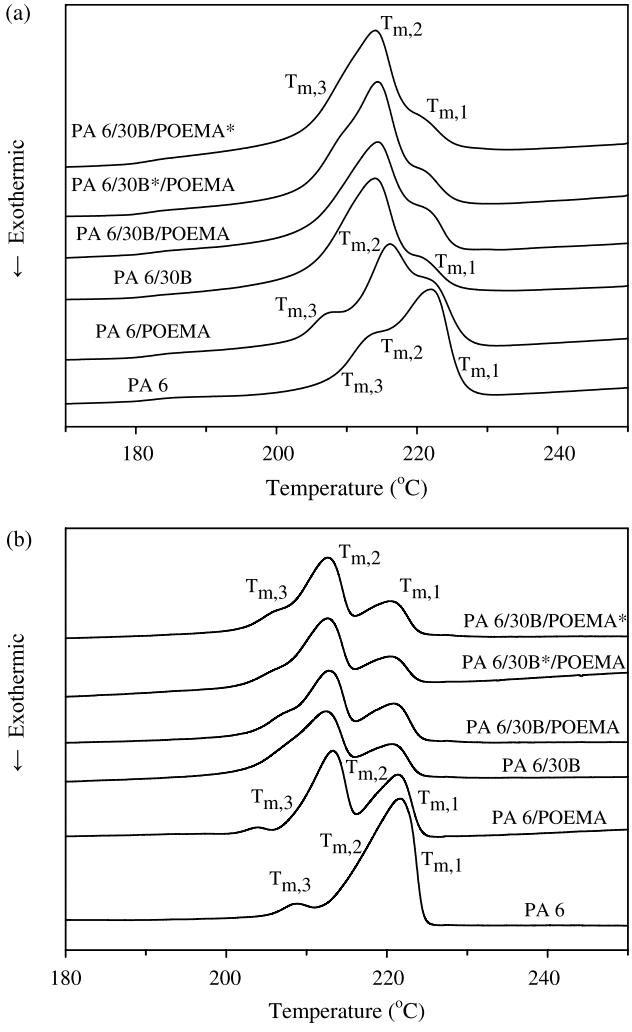

Fig. 7. DSC heating thermograms of 40 °C/min-cooled samples: (a) at 40 °C/min heating rate; (b) at 5 °C/min heating rate.

the original shapes of less stable α form melting peak and $T_{m,2}$ peak are actually not easily seen. Nevertheless, the representative (apparent) T_ms and ΔH_ms (melting enthalpy) determined from Fig. 6(b) are listed in Table 2.

Fig. 7 depicts the melting behaviors of 40 °C/min-cooled samples under 40 °C/min and 5 °C/min heating rates, respectively. These samples exhibit slightly more complex melting behaviors than previous samples. In addition to the $T_{m,1}$ and $T_{m,2}$ peaks, a lower melting temperature shoulder (denoted $T_{m,3}$) on the left-hand side of $T_{m,2}$ peak becomes discernible for most of the thermograms. In some cases (e.g. the neat PA 6 heated at 40 °C/min) the $T_{m,3}$ peak is not so evident, which can be ascribed to the closely overlapping of $T_{m,3}$ peak and $T_{m,2}$ peak. Regarding the origin of $T_{m,3}$ peak, it is believed to belong to the less stable α form crystals discussed above, which transformed into the more stable α form crystals, causing the $T_{m,1}$ peaks, through the 'melting-recrystallization' process during the heating scans. From the above DSC analysis, it could be concluded that the addition of 30B obviously affected the melting behavior of PA 6. The further addition of POEMA influenced the melting behavior of PA 6/30B nanocomposite slightly.

3.4. Thermal stability

The TGA scanned results of neat PA 6, POEMA, and the nanocomposites/blend are shown in Fig. 8(a). Three main features are worthy noting. First, all of the samples displayed single-step degradation process, with POEMA exhibiting the most thermal stability. For instance, POEMA started to degrade around 410 °C, whereas the degradation temperatures for the other samples were below 380 °C. Second, in the 380–430 °C temperature range, the degradation behavior of all samples, except for POEMA, was similar to one another. This result implies that the degradation of PA 6 was affected little by the inclusions of 30B and/or POEMA in this temperature region. Third, as the temperature was above 430 °C, the nanocomposites/blend started to degrade slower than neat PA 6, indicating the PA6 thermal stability enhancement after adding 30B and/or POEMA. Moreover, in the high temperature region, the thermal stability differences among

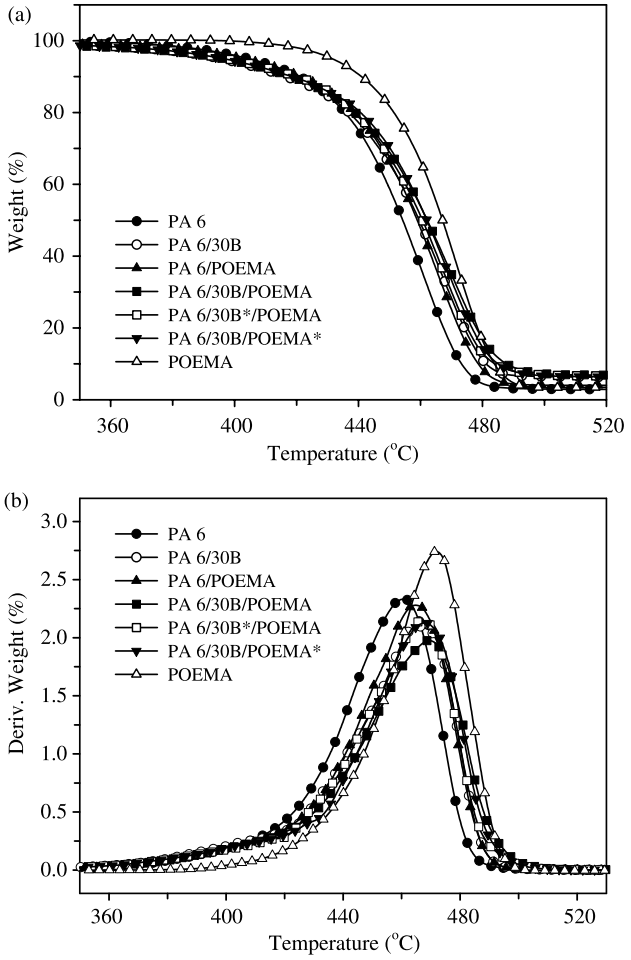

Fig. 8. (a) TGA decomposition curves for the samples; (b) DTGA curves for the samples.

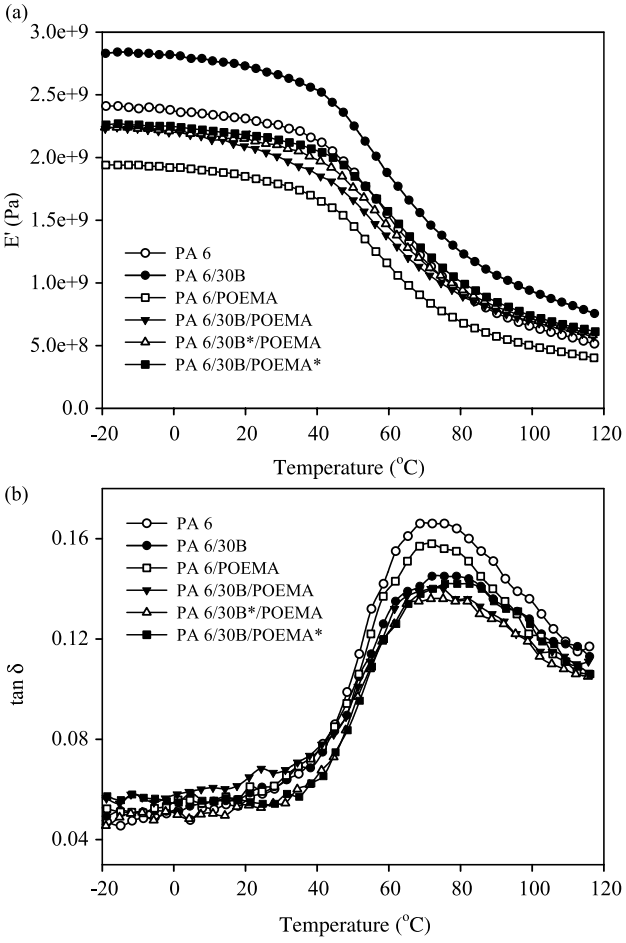

Fig. 9. (a) DMA results of E' vs. temperature for the samples; (b) DMA results of tan δ vs. temperature for the samples.

the nanocomposites/blend were trivial. The observation of similar degradation behavior exhibited by the nanocomposites could be attributed to their comparable 30B/POEMA dispersion status within the PA 6 matrix. The thermal stability enhancement of PA 6 after adding 5 wt% of 30B was a consequence of the nano-scaled dispersion of layered 30B, which resulted in oxygen and heat permeability reductions in the PA 6 matrix during the heating scans. The fact that 30B platelets caused slower decomposed smaller molecule escape should be taken into account. The corresponding derivative TGA (DTGA) results are shown in Fig. 8(b). The peak temperature (T_{max}, temperature at the maximum weight loss rate) follows the order of POEMA > nanocomposites > PA 6/POEMA blend > neat PA 6. These values are listed in Table 2. Further noted is that the peak height of each curve decreases with the additions of 30B and/or POEMA. These results also suggest the thermal stability enhancement of PA 6 in nanocomposites.

3.5. Mechanical properties

Dynamic mechanical properties can reveal useful information about the viscoelastic behaviors of the investigated samples. Fig. 9(a) depicts the storage modulus (E') as a function of temperature for the prepared samples. These samples exhibited similar decreasing E' trends with increasing temperature. This behavior was due to the increase in segmental polymer chain motion with temperature. In the 45–75 °C range, the dramatic E' drop demonstrated the glass transition of PA 6. Worth noting is that the PA 6/30B nanocomposite showed higher E' values, up to 1.4 times those of neat PA 6. This evident E' reinforcement is ascribed to the nano-scaled dispersion of 30B within the PA 6 matrix. In contrast, for the PA 6/POEMA blend, the E' values were ca. 20% lower than those of neat PA 6, and were the lowest among the samples. This result was caused by the elastomeric nature of POEMA. As for the three different-processed nanocomposites including both 30B and POEMA, their E' values were lower than those of neat PA 6 when the temperature was below the glass transition region. This behavior suggests that POEMA played a more important role than 30B in controlling the E' of the samples in the low temperature region. Conversely, when the temperature was above the glass transition region, the three nanocomposites showed higher E' values than neat PA 6. This result indicates the evident reinforcing role that 30B played at higher temperatures. While comparing these three

nanocomposites, only minor differences in E' values were observed. Fig. 9(b) shows the loss tangent (tan δ) versus temperature for the samples. The dynamic relaxation peak, corresponding to the glass transition of PA 6, is observed for each sample. It is found that the peak temperatures (i.e., glass transition temperatures, T_gs) of the nanocomposites were about 3 °C higher than those for neat PA 6 and the blend. Moreover, the nanocomposites exhibited lower relaxation peak heights compared with neat PA 6 and the blend. These tan δ results imply that 30B was intercalated/exfoliated into the polymeric matrix, which resulted in a retardation in polymer chain mobility with temperature and, hence, lower hysteresis loss.

In addition to the dynamic mechanical properties, tensile properties of the samples were measured. The measured Young's modulus (YM), tensile strength (TS) and elongation at break (EB) are listed in Table 2. It is evident that adding 30B effectively increased the Young's modulus and tensile strength of PA 6 (cf. PA 6/30B nanocomposite). However, the elongation at break was inversely affected. With the incorporation of POEMA into the PA 6 matrix (cf. PA 6/POEMA blend), the tensile properties declined, stemming from the elastomeric nature of POEMA. For the three different-processed PA 6/30B/POEMA nanocomposites, the tensile properties fell between those of neat PA 6 and PA 6/30B nanocomposite. The tensile properties differences among the three samples were marginal.

Izod impact tests were carried out to determine the effects of adding 30B and/or POEMA on the samples toughness. The results are included in Table 2 which reveals that after adding 30B the impact strength (IS) of PA 6 decreased ca. 40%, reaching a value of 22.8 J/m. Conversely, the incorporation of POEMA resulted in a 2.77 times increase in PA 6 impact strength (up to 104.8 J/m), indicating an apparently toughening effect. The reason for this remarkable enhancement is believed to be associated with the interactions (compatibility) between the MA portion of POEMA and the amino group of PA 6. For the three different-processed nanocomposites, balanced impact strengths were observed. Their impact strengths showed an average increase of 1.5 times that of neat PA 6. Note that the PA 6/30B*/POEMA nanocomposite exhibited a slightly higher impact strength than the other two samples. The reason for this behavior is not clear at this moment. It might be caused by a slightly phase morphology difference, which was not noticed. To justify this explanation, supplementary experiments are being conducted.

4. Conclusions

This study investigated the dispersibility of a commercial O-MMT (30B) within a PA 6 matrix in the absence or presence of a POEMA toughener. The thermal/mechanical properties of the melt-mixed samples were determined as well. The influence of different mixing sequences on the phase morphology and thermal/mechanical properties of the PA 6/30B/POEMA composites was also evaluated. XRD, SEM/EDS, and TEM results indicated that the layered 30B was exfoliated (or at least intercalated) in the prepared composites. The PA 6-based nanocomposites were achieved irrespective of the processing sequence employed. The incorporation of 30B and/or POEMA would promote the formation of γ form PA 6 crystals, with 30B exhibiting higher effectiveness. The crystallization kinetics of PA 6 was evidently altered as 30B was added. This is mainly due to the formation of different polymorphs. The complex DSC melting behaviors observed for the samples were attributed to different polymorphs and/or the occurrence of 'melting-recrystallization-remelting' process. The TGA data confirmed the moderate thermal stability enhancement of PA 6 after adding 30B and/or POEMA. The storage/Young's moduli and tensile strength of PA 6 increased with the inclusion of 30B. However, the addition of POEMA produced a decrease in these properties. Conversely, 30B and POEMA additions produced a reverse effect on the PA 6 toughness. The different-processed PA 6/30B/POEMA nanocomposites presented balanced mechanical properties between those of neat PA 6 and PA 6/30 nanocomposite.

Acknowledgements

The authors would like to thank the National Science Council of the Republic of China (Taiwan) for financially supporting this research under contract number NSC-91-2622-E-197-006-CC3.

References

[1] Usuki A, Kojima Y, Kawasumi M, Okada A, Fukushima Y, Kurauchi T, et al. J Mater Res 1993;8:1179.
[2] Kojima Y, Usuki A, Kawasumi M, Okada A, Kurauchi T, Kamigaito O. J Polym Sci, Polym Chem Ed 1993;31:983.
[3] Heinemann J, Reichert P, Thomann R, Mulhaupt R. Macromol Rapid Commun 1999;20:423.
[4] Gopakumar TG, Lee JA, Kontopoulou M, Parent JS. Polymer 2002;43:5483.
[5] Zhang Q, Wang Y, Fu Q. J Polym Sci, Polym Phys Ed 2002;41:1.
[6] Chiu FC, Lai SM, Chen JW, Chu PH. J Polym Sci, Polym Phys Ed 2004;42:4139.
[7] Kornmann X, Thomann R, Mulhaupt R, Finter J, Berglund LA. Polym Eng Sci 2002;42:1815.
[8] Ke Y, Long C, Qi Z. J Appl Polym Sci 1999;71:1139.
[9] Ou CF, Ho MT, Lin JR. J Polym Res 2003;10:127.
[10] Hu X, Lesser AJ. J Polym Sci, Polym Phys Ed 2003;41:2275.
[11] Li X, Kang T, Cho WJ, Lee JK, Ha CS. Macromol Rapid Commun 2001;22:1306.
[12] Lincoln DM, Vaia RA, Wang ZG, Hsiao BS. Polymer 2001;42:1621.
[13] Zhang QX, Yu ZZ, Yang M, Ma J, Mai YW. J Polym Sci, Polym Phys Ed 2003;41:2861.
[14] Wu TM, Liao CS. Macromol Chem Phys 2000;201:2820.
[15] Vaia RA, Jandt KD, Kramer EJ, Giannelis EP. Macromolecules 1995;28:8080.
[16] Pourabas B, Raeesi V. Polymer 2005;46:5533.
[17] Mishra JK, Kim II H, Ha CS. Macromol Rapid Commun 2003;24:671.
[18] Liu L, Qi Z, Zhu X. J Appl Polym Sci 1999;71:1133.
[19] Fornes TD, Yoon PJ, Keskkula H, Paul DR. Polymer 2001;42:9929.
[20] Cho JW, Paul DR. Polymer 2001;42:1083.
[21] Liu TX, Liu ZH, Ma KX, Shen L, Zeng KY, He CB. Compos Sci Technol 2003;63:331.

[22] Lincoln DM, Vaia RA, Wang ZG, Hsiao BS, Krishnamoorti R. Polymer 2001;42:9975.
[23] Tjong SC, Bao SP. J Polym Sci, Polym Phys Ed 2004;42:2878.
[24] Chow WS, Mohd Ishak ZA, Karger-Kocsis J, Apostolov AA, Ishiaku US. Polymer 2003;44:7427.
[25] Tang Y, Hu Y, Zhang R, Gui Z, Wang Z, Chen Z, Fan W. Polymer 2004; 45:5317.
[26] Li Y, Shimizu H. Polymer 2004;45:7381.
[27] Chow WS, Bakar AA, Mohd Ishak ZA, Karger-Kocsis J, Ishiaku US. Eur Polym J 2005;41:687.
[28] Yu ZZ, Ou YC, Hu GH. J Appl Polym Sci 1998;69:1711.
[29] Yu ZZ, Ke YC, Ou YC, Hu GH. J Appl Polym Sci 2000;76: 1285.
[30] Sengupta R, Bandyopadhyay A, Sabharwal S, Chaki TK, Bhowmick AK. Polymer 2005;46:3343.
[31] Ramesh C, Gowd EB. Macromolecules 2001;34:3308.